PAPER

Head Tissue Heterogeneity Required in Computational Dosimetry for Portable Telephones

Jianqing WANG[†] and Osamu FUJIWARA[†], *Regular Members*

SUMMARY　The head tissue heterogeneity required in the spatial peak specific absorption rate (SAR) assessment for portable telephones was investigated by using the FDTD method in conjunction with an MRI-based human head model. The tissue heterogeneity of the head model was changed from one type of tissue to 17 types of tissue. The results showed that, at 900 MHz and 2 GHz, the homogeneous modeling results in an underestimate about 20% for the $\lambda/2$ monopole antenna portable telephones and an overestimate to the same extent for the $\lambda/4$ monopole or helical antenna portable telephones. A head model with a simple skin-fat-muscle-bone-brain structure seems to be sufficient to obtain a fairly accurate one-gram or ten-gram averaged spatial peak SAR value in computational dosimetry for portable telephone compliance.

key words: *computational dosimetry, head tissue heterogeneity, portable telephone, FDTD*

1. Introduction

With the recent rapid increase in the use of portable telephones, safety guidelines for protecting human beings from the radio frequency exposure have been issued in various countries [1]–[3]. Especially, since 1996, the U.S. Federal Communication Commission (FCC) has required the routine specific absorption rate (SAR) evaluation prior to device authorization or use [4]. According to the FCC regulation, any portable telephone has to be evaluated with respect to the SAR limit using either phantom measurement or computer simulation. For computer simulation, human head models being usually derived from magnetic resonance imaging (MRI) or computed tomography (CT) scans are used. However, the derived head models were reported with various tissue complexities, ranged from several to dozens of tissue types [5]–[8], while an actual head anatomically has over 800 tissue types. Hombach et al. and Meier et al. numerically analyzed the interaction between $\lambda/2$ dipole antennas and human head models and they both concluded that homogeneous modeling of human head is suited for assessing the spatial peak SAR, although it is hard to avoid an overestimate which sometimes may exceed 40% [6], [7]. To what extent the tissue structure heterogeneity gives a reasonable SAR assessment remains unclear. Moreover, due to the difference in the interaction between different

antenna types and the human head, the antenna type should affect the peak SAR, while its dependence on tissue heterogeneity also remains unclear.

　The objective of this paper is to investigate the role of head tissue heterogeneity in the peak SAR assessment. An our newly developed MRI-based head model [9], [10] was employed for this aim. The head model has a high tissue heterogeneity of 17 tissue types. Based on the same MRI data, 16 other head models with tissue complexities from one tissue type to 16 tissue types were also developed. The finite-difference time-domain (FDTD) method was used to calculate the spatial peak SARs in the 17 head models for the two most popular antennas and two frequency bands. The two most popular antennas were a monopole and a helix both mounted on a plastic-covered metal box. The two frequency bands were 900 MHz and 2 GHz, which are being employed and will be employed in the near future in Japan, respectively.

2. Models and Analysis Method

2.1 MRI Based Head Model

The raw MRI data were taken from a Japanese adult head (male, 23 years old), which consists of 115 slices with 2 mm space in the axial plane. Each MRI slice was a 256×256 pixel and 9-bit grey scale image. The grey scale data of MRI images were interpreted into tissue types, which is known as a process of segmentation. The segmentation was performed under the guidance of a medical doctor. At first, the grey scale images were rescaled to produce cubic voxels of 2 mm. Then the images were segmented unambiguously as belonging to one of 17 different tissue types by assigning each 2 mm cube voxel to a RGB code, which identifies the discrete tissue type of that particular voxel. This process was performed manually with the aid of a commercial software Adobe Photoshop. Figure 1 shows the head model, a mid-sagittal vertical cross-section and a horizontal cross-section through the eyes of the head model. The 16 other head models with tissue complexities from one tissue type to 16 tissue types were developed based on the same MRI data. For example, the one-tissue model was composed of the brain tissue (whose dielectric properties were assumed to be the averages of the grey matter and white matter), the two-tissue model

was composed of the skin and brain tissue, the three-tissue model was composed of the skin, bone and brain tissue, and so on. Table 1 shows the composition of each model as well as electrical properties for each tissue [12] where ρ is the mass density, and ε_r and σ are the relative permittivity and conductivity, respectively. It is worthy noting that the 2 mm cubic cells are 1/20 and 1/9 of the smallest wavelength in the tissue at 900 MHz and 2 GHz, respectively.

2.2 Modeling of Portable Telephone with a Monopole Antenna

Based on [11], the handset of portable telephone was modeled as a dielectric covered rectangular metal box

Fig. 1 MRI-based head model. (a) appearance, (b) mid-sagittal vertical cross-section, (c) horizontal cross-section through the eyes.

with a length of 12.4 cm, a width of 4.4 cm and a thickness of 2.4 cm. The metal box was covered with a dielectric insulator of 2 mm thickness and ε_r=2.0. A $\lambda/2$ or $\lambda/4$ monopole antenna was mounted on the top of the handset, in the front of the 4.4 cm side and 2 cm far from the edge of the 2.4 cm side. This corresponded to a distance of 2 cm between the monopole and the the ear because the handset was barely touching the ear. The radius of the monopole was 0.5 mm, which was approached by the thin-wire approximation [11] for considering the effect of a wire with a radius smaller than the FDTD cell dimensions. δ-gap feeding was employed to excite the monopole antenna.

2.3 Modeling of Portable Telephone with a Helical Antenna

The helical antenna, having a pitch S=2 mm, a diameter D=4 mm and a length L=1.4 cm at 900 MHz and L=1.6 cm at 2 GHz, was mounted on the top of the same handset described above. According to Lazzi and Gandhi's proposal for modeling a helical antenna in [8], a rectangular stack, as shown in Fig. 2, was used to reproduce the fields generated by the helix. Referring to Fig. 2(b), one layer of the stack has an equivalent dipole and an equivalent loop. Denoting the current in the equivalent dipole as I'_d, we can replace it with a displacement current, and have the equivalent electric field E_z in lieu of I'_d, which is expressed as

$$E_z = \frac{I'_d \cdot 1/j\omega C}{s} = \frac{I'_d}{j\omega\varepsilon_0 D^2} \tag{1}$$

where C is the capacitance between the layer, being given by $\varepsilon_0 D^2/s$.

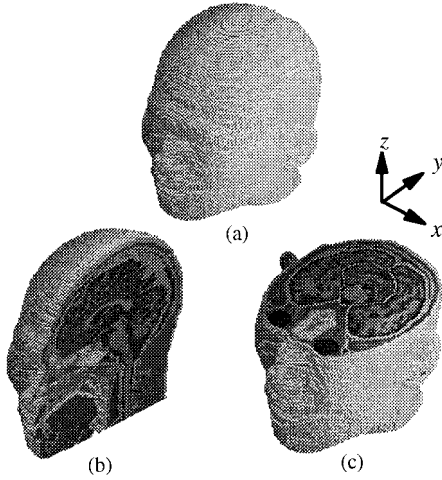On the other hand, denoting the current in the

Table 1 Dielectric properties of tissue and composition of head models.

Tissue type	ρ [kg/m^3]	900 MHz		2 GHz		n**
		ε_r	σ [S/m]	ε_r	σ [S/m]	
brain*	1030.0	45.81	0.77	43.21	1.26	1
skin	1010.0	41.41	0.87	38.57	1.27	2
bone	1850.0	16.62	0.24	15.37	0.48	3
fat	920.0	11.33	0.11	10.96	0.21	4
muscle	1040.0	55.96	0.97	54.17	1.51	5
dura	1030.0	44.43	0.96	42.62	1.42	6
CSF	1010.0	68.64	2.41	66.91	3.07	7
cartilage	1100.0	42.65	0.78	39.76	1.42	8
grey matter	1030.0	52.72	0.94	49.69	1.51	9
white matter	1030.0	38.89	0.59	36.73	1.00	9
parotid gland	1050.0	60.55	1.21	58.27	1.83	10
eye humour	1010.0	55.27	1.17	68.47	2.16	11
lens	1100.0	41.21	0.64	39.78	1.06	12
bone marrow	1030.0	11.27	0.23	10.56	0.38	13
blood	1060.0	61.36	1.54	59.02	2.19	14
mucous membrane	1010.0	46.08	0.84	43.52	1.34	15
sclera	1170.0	55.27	1.27	53.27	1.72	16
cornea	1050.0	55.23	1.39	52.39	1.98	17

* Average of the grey matter and white matter.
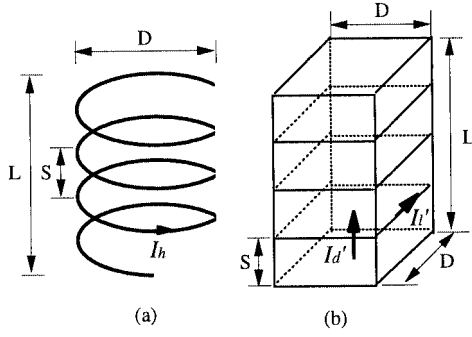** n stands for the number of tissue constitutes a head model.

Fig. 2 (a) Size of helical antenna, (b) stack used to model the helical antenna. The stack is composed of several layers. Each layer has a square area with one side equal to the diameter D and a height equal to the pitch S of the helical antenna.

equivalent loop as I'_l, from Biot-Savart's law, we can obtain the equivalent magnetic field related to the current I'_l in the center of the same layer, which is given as

$$H_z = \oint \frac{I'_l dl' \sin\phi}{4\pi R^2} = \frac{4}{\sqrt{2}\pi} \frac{I'_l}{D} \tag{2}$$

where R is the distance from the current element dl' to the center of the layer, ϕ is the angle between the direction of the current and the vector from the element to the center of the layer, and the integration is carried out along the boundary line of the layer. Thus, for one layer of the stack, we have

$$\frac{E_z}{H_z} = \frac{I'_d}{I'_l} \frac{\sqrt{2}\pi}{j4\omega\varepsilon_0 D}. \tag{3}$$

Since each layer of the stack had the same height as the pitch of the helix, the currents I'_d was equal to the actual helix current I_h. Moreover, since the actual loop of the helix has a circular shape, for inducing the same magnetic field in the center of the loop, the current I'_l should be related to actual helix current I_h by $I'_l = \frac{\sqrt{2}\pi}{4} I_h$. Thus Eq. (3) can be rewritten as

$$\frac{E_z}{H_z} = \frac{1}{j\omega\varepsilon_0 D} \tag{4}^\dagger$$

The excitation of the helical antenna was performed by using sinusoidal E_z and H_z according to the above relationship.

3. Results and Discussion

Figures 3 and 4 show the dependence of the one-gram and ten-gram averaged spatial peak SAR on tissue heterogeneity. The portable telephones were set to have a vertical alignment at the side of the head by the ear. The hand was simply modeled with 2/3 muscle-equivalent material being 8 cm wide and 2 cm thick and wrapped around three sides of the lower part of the handset. The one-gram averaged and ten-gram averaged spatial peak SARs were obtained over a 1 cm^3 and
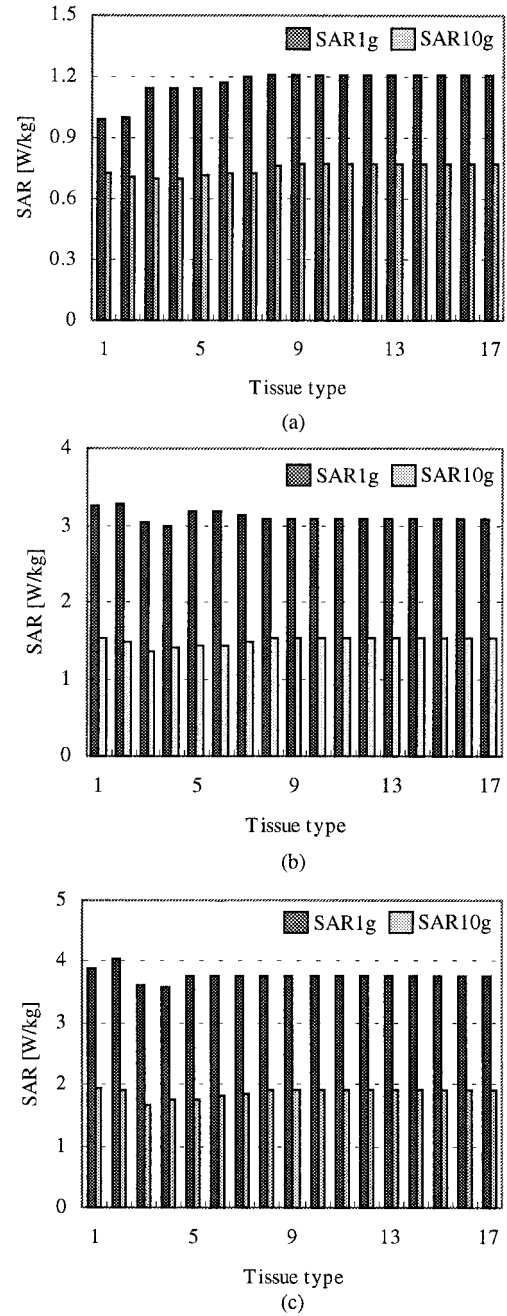

Fig. 3 Dependence of the one-gram and ten-gram averaged spatial peak SAR on tissue complexity at 900 MHz. (a) $\lambda/2$ monopole antenna, (b) $\lambda/4$ monopole antenna, (c) helical antenna.

2.2 cm^3 cubics, respectively, which did not include air.

---

†This is somewhat different from the relationship $E_z/H_z = 4/(j\omega\varepsilon_0\pi D)$ derived by Lazzi and Gandhi in [8]. The reason is that H_z in Eq. (2) was approximated as I'_l/D in [8], although the integral should be $4I'_l/\sqrt{2}\pi D$. This approximation yielded a H_z value of 10% $(1 - 4/\sqrt{2}\pi)$ less than the actual H_z value. The corresponding differences for the one-gram and ten-gram averaged spatial peak SARs due to this approximation were within 0.1% according to our numerical results at 900 MHz.
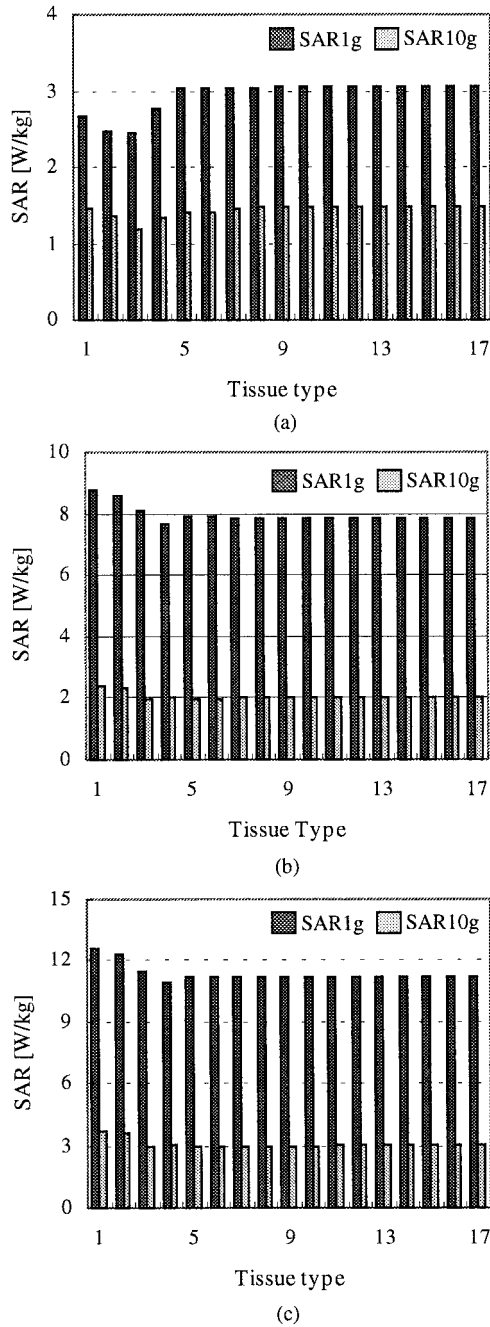
Fig. 4 Dependence of the one-gram and ten-gram averaged spatial peak SAR on tissue complexity at 2 GHz. (a) $\lambda/2$ monopole antenna, (b) $\lambda/4$ monopole antenna, (c) helical antenna.

All of the results were normalized to an antenna output of 1 W. The antenna outputs, for both the monopole antenna and the helical antenna, were obtained from the sum of the power absorbed in the head and hand and the power radiated to the far field. The radiated power was calculated by integrating the normal components of the Poynting vector over a surface completely surrounding the configuration of analysis. As can be seen from the results, for the $\lambda/2$ monopole antenna

portable telephones, the one-tissue model exhibited an underestimate feature at the two considered frequencies. With respect to the 17-tissue model, the one-tissue model gave underestimates of 18% at 900 MHz and 13% at 2 GHz for the one-gram averaged spatial peak SAR. The similar feature can be observed for the ten-gram averaged spatial peak SAR, but the underestimated levels were much smaller with respect to the one-gram averaged values. Especially at 2 GHz, the ten-gram averaged peak SAR for the one-tissue model was almost the same as that for the 17-tissue model. However, for the $\lambda/4$ monopole and helical antenna portable telephones, the one-tissue model gave an upper bound for the one-gram and ten-gram averaged spatial peak SAR. With respect to the 17-tissue model, at 900 MHz, the one-tissue model gave an overestimate within 5%, while at 2 GHz, the one-tissue model gave overestimates up to 12% and 20% for the one-gram and ten-gram averaged spatial peak SARs, respectively. It should be noted that the results for $\lambda/4$ monopole or helical antennas support the finding in [6] that a homogeneous head overestimates the peak SAR, but it is not true for the $\lambda/2$ monopole antenna.

From these results the dependence of the peak SAR on tissue heterogeneity seems to be antenna-dependent. This may be explained from the different composition of tissue in the ear region and on the upper side of the ear. Figure 5 shows the SAR distributions in the zx plane for the $\lambda/2$ monopole antenna and helical antenna at 900 MHz. For the $\lambda/2$ monopole antenna the peak current appeared at the center of the monopole, which resulted in that the main EM absorption area was on the upper side of the ear. The volume of brain tissue is large in this region. However, due to the short length of $\lambda/4$ monopole and helical antenna, the currents in these cases concentrated at the bottom of the antenna and the upper part of the handset, which resulted in a concentrated EM absorption in the ear region with a more complex tissue composition.

Furthermore, from Figs. 3 and 4, when the tissue types were larger than 5, the peak SAR approximately converged to the value for the 17-tissue model. The 5-tissue model, i.e., the skin-fat-muscle-bone-brain model, was found to have a difference for the one-gram and ten-gram averaged spatial peak SAR within 5% with respect to the 17-tissue model. This relationship holds for both the monopole and the helical antennas at both 900 MHz and 2 GHz. By comparing the SAR profiles for the head models with different tissue heterogeneity, as shown in Fig. 6, it is obvious that the SAR profiles close to the head surface, that determine the gram-averaged spatial peak SAR, have a similarity between the 5-tissue model and the 17-tissue model. This phenomenon attributes to the fact that the skin, fat, muscle, bone and brain are the main tissue types in the exposed region of head.

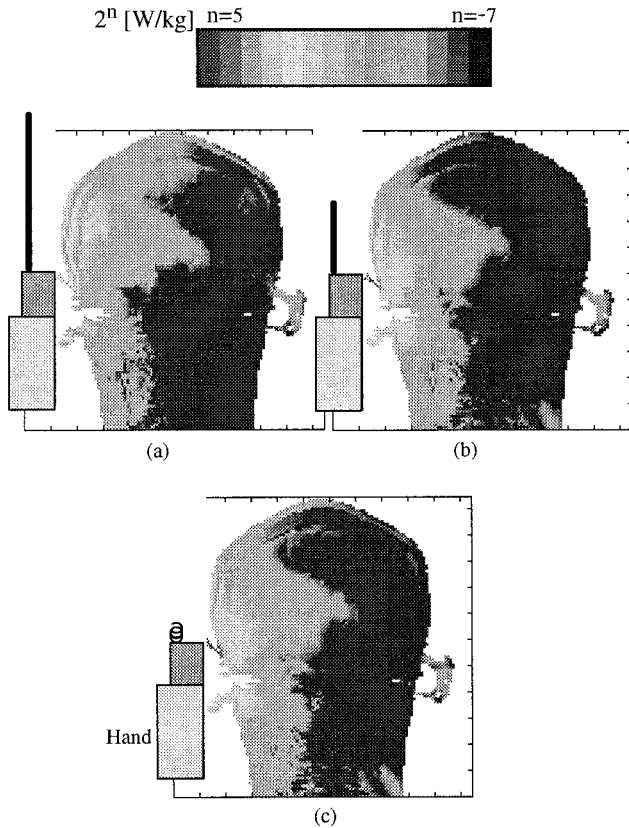These findings lead to a conclusion that a head

Fig. 5 SAR distributions in the zx plane at 2 GHz. (a) $\lambda/2$ monopole antenna, (b) $\lambda/4$ monopole antenna, (c) helical antenna.
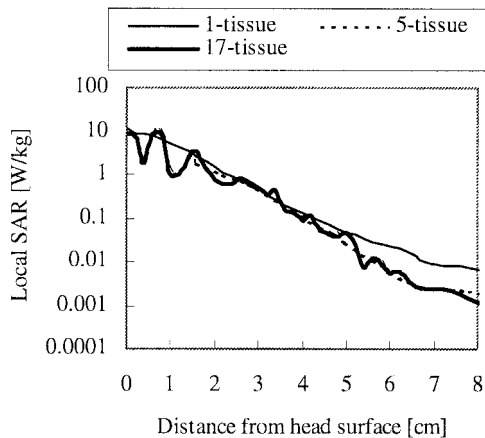

Fig. 6 SAR profiles along the x axis for a helical antenna at 2 GHz.

model with a simple skin-fat-muscle-bone-brain structure is sufficient to derive a fairly accurate peak SAR value in computational dosimetry for portable telephone compliance.

The same conclusion applies also to the SAR averaged over the whole head. Figure 7 shows the dependence of the whole-head-averaged SAR on the tissue complexity for the $\lambda/2$ monopole antenna and helical
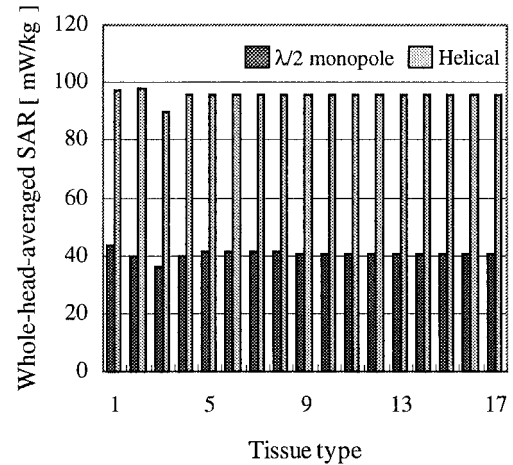

Fig. 7 Dependence of the whole-head-averaged SAR on tissue complexity at 2 GHz.

antenna portable telephones at 2 GHz. It is found that the average SAR for the 5-tissue model obviously converges to that for the 17-tissue model.

4. Conclusion

The head tissue heterogeneity required in the peak SAR assessment for portable telephones was investigated by using the FDTD method in conjunction with an MRI-based human head model. The tissue heterogeneity of the head model was changed from one type of tissue to 17 types of tissue. The investigated frequencies were 900 MHz and 2 GHz, and the investigated antenna types were popular monopole and helical antennas, both mounted on a dielectric covered metal box. The results showed that the homogeneous modeling results in an underestimate about 20% for the $\lambda/2$ monopole antenna portable telephones and an overestimate to the same extent for the $\lambda/4$ monopole and helical antenna portable telephones. A head model with a simple skin-fat-muscle-bone-brain structure gives almost the same peak SAR value as a highly complex 17-tissue model, which suggests that the 5-tissue head model is sufficient to obtain a fairly accurate peak SAR in computational dosimetry for portable telephone compliance.

A further subject is to investigate the head tissue heterogeneity required in the dosimetry analysis for children because the tissue structure and dielectric properties may change during the development from the newly born to the adult. Unfortunately, there are no measurement data on the dielectric properties for children available in the literature. To develop an anatomically realistic child head model and evaluate the dielectric properties for children are prerequisite.

References

[1] American National Standards Institute, "Safety levels with respect to exposure to radio frequency electromagnetic fields,

3 kHz to 300 GHz," ANSI/IEEE C95.1-1992.

[2] International Commission on Non-Ionizing Radiation Protection, "ICNIRP statement—Health issues related to the use of hand-held radiotelephones and base transmitters," Health Physics, vol.70, no.4, pp.587–593, April 1996.

[3] Report of Telecommunications Technology Council for the Ministry of Posts and Telecommunications, Deliberation no.89, "Radio-radiation protection guidelines for human exposure to electromagnetic fields," Tokyo, 1997.

[4] Federal Communications Commission, "Report and order: guidelines for evaluating the environmental effects of radiofrequency radiation," FCC 96-326, Washington DC, 1996.

[5] M. Okoniewski and M.A. Stuchly, "A study of the handset antenna and human body interaction," IEEE Trans. Microwave Theory & Tech., vol.44, no.10, pp.1855–1864, Oct. 1996.

[6] V. Hombach, K. Meier, M. Burkhardt, E. Kuhn, and N. Kuster, "The dependence of EM energy absorption upon human head modeling at 900 MHz," IEEE Trans. Microwave Theory & Tech., vol.44, no.10, pp.1865–1873, Oct. 1996.

[7] K. Meier, V. Hombach, R. Kastle, R.Y.S. Tay, and N. Kuster, "The dependence of EM energy absorption upon human head modeling at 1800 MHz," IEEE Trans. Microwave Theory & Tech., vol.45, no.11, pp.2058–2062, Nov. 1997.

[8] G. Lazzi and O.P. Gandhi, "On modeling and personal dosimetry of cellular telephone helical antennas with the FDTD code," IEEE Trans. Antennas & Propagat., vol.46, no.4, pp.525–529, April 1998.

[9] T. Ushimoto, J. Wang, and O. Fujiwara, "Dosimetry and its dependence of irradiation direction in MRI based head model for 1.5 GHz microwave far-fields," IEICE Technical Report, EMCJ99-16, June 1999.

[10] J. Wang and O. Fujiwara, "FDTD analysis of dosimetry in human head model for a helical antenna portable telephone," IEICE Trans. Commun., vol.E83-B, no.3, March 2000.

[11] L. Chen, T. Uno, S. Adachi, and R. Luebbers, "FDTD analysis of a monopole antenna on a conducting box with a layer of dielectric," IEICE Trans. Commun., vol.E76-B, no.12, pp.1583–1586, Dec. 1993.

[12] C. Gabriel, "Compilation of the dielectric properties of body tissues at RF and microwave frequencies," Brooks Air Force Technical Report AL/OE-TR-1996-0037, 1996.

Osamu Fujiwara received the B.E. degree in electronic engineering from Nagoya Institute of Technology, Nagoya, Japan, in 1971, and the M.E. and the D.E. degrees in electrical engineering from Nagoya University, Nagoya, Japan, in 1973 and in 1980, respectively. From 1973 to 1976, he worked in the Central Research Laboratory, Hitachi, Ltd., Kokubunji, Japan, where he was engaged in research and development of system packaging designs for computers. From 1980 to 1984 he was with the Department of Electrical Engineering at Nagoya University. In 1984 he moved to the Department of Electrical and Computer Engineering at Nagoya Institute of Technology, where he is presently a professor. His research interests include measurement and control of electromagnetic interference due to discharge, bioelectromagnetics and other related areas of electromagnetic compatibility. Dr. Fujiwara is a member of the Institute of Electrical Engineers of Japan and of the Institute of Electrical and Electronics Engineers of America.

Jianqing Wang received the B.E. degree in electronic engineering from Beijing Institute of Technology, Beijing, China, in 1984, and the M.E. and D.E. degrees in electrical and communication engineering from Tohoku University, Sendai, Japan, in 1988 and 1991, respectively. After he worked as a Research Associate at Tohoku University and a Research Engineer at Sophia Systems Co., Ltd., he moved to the Department of Electrical and Computer Engineering at Nagoya Institute of Technology, Nagoya, Japan, in 1997, where he is currently an Assistant Professor. His research interests include electromagnetic compatibility, bioelectromagnetics and digital communications.